

Starburst or Seyfert? Adding a radio and far-infrared perspective to the investigation of activity in composite galaxies

Tanya L. Hill¹

School of Physics, University of Sydney

Charlene A. Heisler²

Research School for Astronomy and Astrophysics, Australian National University

Ray P. Norris and John E. Reynolds

Australia Telescope National Facility

and

Richard W. Hunstead

School of Physics, University of Sydney

ABSTRACT

It was once common to regard Seyfert and starburst galaxies as completely different types of object, but there is growing recognition that these classifications refer to the extremes of a continuous spectrum of galaxy types. In a previous study we investigated a sample of galaxies with ambiguous optical emission-line ratios and concluded from near-infrared spectroscopic observations that the sample consisted of composite galaxies, containing both a starburst and an active galactic nucleus (AGN). We now extend our study using radio synthesis and long-baseline interferometer observations made with the Australia Telescope, together with far-infrared IRAS observations, to discuss the relative contribution of starburst and AGN components to the overall luminosity of the composite galaxies. We find that only a small fraction of the radio emission (< 10%) can be attributed to an AGN, and that the majority of the far-infrared emission (> 90%) is probably due to the starburst component. We also show that an AGN contribution to the optical emission of as little as 10% is sufficient to account for the ambiguous line-ratio diagnostics.

Subject headings: galaxies: active — galaxies: Seyfert — galaxies: starburst

1. Introduction

The possible existence of a relationship between massive star formation and an active galactic nucleus (AGN) is a long standing, controversial issue. An increasing number of galaxies have been shown

¹Present address: Melbourne Planetarium, 2 Booker St, Spotswood, VIC, 3015, Australia; email:thill@museum.vic.gov.au

²This paper is dedicated to the memory of Charlene Heisler (deceased, 28 October 1999).

to contain both intense star formation, typical of a starburst galaxy, as well as a non-thermal ionising source, attributed to an AGN. Well known examples of such composite galaxies are NGC 1068 (Thatte *et al.* 1997), NGC 7469 (Genzel *et al.* 1995), Mrk 477 (Heckman *et al.* 1997) and Circinus (Oliva *et al.* 1995), all of which contain, in addition to a Seyfert nucleus, circumnuclear star formation that contributes significantly to the total luminosity. In many such cases, the composite nature of the galaxies is based on optical and NIR ob-

servations. However, radio observations can also be a powerful tool for distinguishing starburst and AGN activity.

In general, galaxies dominated by starbursts exhibit diffuse radio emission as the result of synchrotron radiation associated with supernova remnants and cosmic rays (Sramek & Weedman 1986). Seyfert galaxies, on the other hand, generally exhibit more compact emission or, in the more radio-energetic cases, linear structures, identifiable as jets and radio lobes (Wilson *et al.* 1991). The use of radio morphology to distinguish the dominant activity within galaxies is well established (Norris *et al.* 1988a; Wilson 1988; Crawford *et al.* 1996). As one example, NGC 1068, a known composite galaxy, has been observed in the radio to contain both diffuse emission, presumably as a result of star formation, and linear structure, attributed to a jet (Wilson & Ulvestad 1982; Wynn-Williams *et al.* 1985; Gallimore *et al.* 1997).

As a step towards exploring the possible relationship between starburst and Seyfert activity within a homogeneous data set, we have formed a sample of galaxies that are composite in nature. The galaxies were chosen on the basis of optical spectroscopy and investigated further using near-infrared (NIR) spectroscopy (Hill *et al.* 1999: Paper 1). In this previous study, we found only one galaxy, from a sample of 12, to be dominated in the optical/NIR by star formation, with minimal, if any, contribution from an AGN. However, the remaining 11 galaxies show evidence that they are composed of a starburst population and dust heated to temperatures of up to 1000 K by an AGN. In this paper, we present a radio study of the sample in an attempt to place tighter limits on the AGN contribution.

The Australia Telescope Compact Array (ATCA) was used to image our sample at 3 and 6 cm. These data are combined with additional information such as radio spectral indices and far-infrared (FIR) colours to investigate further the nature of the powering source. We also present long-baseline interferometry observations using the Parkes-Tidbinbilla Interferometer (PTI; Norris *et al.* 1988b). PTI is sensitive to structures with sizes $\leq 0.1''$ (corresponding to 40 pc at the mean distance of the sample) at 13 cm and brightness temperatures $> 10^5$ K. PTI will therefore respond to the non-thermal emission from compact cores

of Seyferts with brightness temperatures $\sim 10^8$ K, yet is essentially blind to extended H II regions or supernovae associated with starbursts, which have typical brightness temperatures of 10^4 K. However, recent studies suggest that extremely luminous radio supernovae (RSNe) associated with starbursts may also account for some of the emission detected with PTI (Kewley *et al.* 2000a; Smith *et al.* 1998a).

The sample selection criteria are presented in Section 2. Details of the observations and data reduction for the ATCA and PTI are given in Section 3. Our results are presented and discussed in Section 4, with our conclusions in Section 5. Throughout this paper, we adopt $H_0 = 75 \text{ km s}^{-1} \text{ Mpc}^{-1}$ and $q_0 = 0.5$.

2. Sample Selection

Our sample consists of galaxies, identified in Paper 1, that have characteristics intermediate between starbursts and AGNs based on optical spectroscopy. We used the optical emission-line diagnostic diagrams of Veilleux & Osterbrock (1987), where the emission-line ratios of $[\text{O III}]/\text{H}\beta$, $[\text{N II}]/\text{H}\alpha$, $[\text{S II}]/\text{H}\alpha$ and $[\text{O I}]/\text{H}\alpha$ are compared, to find galaxies that are not clearly identified as either a starburst or AGN. The emission-line ratios used by Veilleux & Osterbrock are generally good discriminators of starbursts and AGNs, because each ratio consists of a forbidden line, which is relatively strong in the partially ionised regions of AGNs, compared with a hydrogen recombination line, which is excited by hot stars formed in starbursts. The galaxies in our sample lie in an intermediate region between the starburst and AGN groupings, either by falling within ± 0.15 dex of the boundary line separating starbursts and Seyferts, or by falling within the domain of starburst galaxies in one diagnostic diagram and within the domain of AGNs in another. The sample was also constrained by a redshift upper limit of $z = 0.035$ and declinations south of $+24^\circ$. Full details of the sample selection are given in Paper 1.

NIR spectroscopy, undertaken in Paper 1, showed that the ambiguous nature of the galaxies was not limited to optical emission but that NIR emission-line ratios also failed to distinguish the galaxies as starburst or AGN. From this, and from further results in Paper 1, we concluded that the

galaxies are composites, containing both a starburst and AGN component.

3. Observations and Reductions

3.1. ATCA

Radio continuum observations were made in 1996 April 8–11, using the Australia Telescope Compact Array in the 6A configuration, which utilises all six antennas and covers east–west baselines from 337 m to 6 km. Observations were made simultaneously at 6 and 3 cm, centred on frequencies of 4.800 and 8.640 GHz respectively, each spanning a bandwidth of 128 MHz. The galaxies were observed in the time-efficient snapshot mode, whereby a number of short observations, or cuts, of each galaxy are made over a wide range of hour angles (Burgess & Hunstead 1995). Between 10–20 cuts, each approximately 10 minutes, were made for every galaxy. Unresolved phase calibrators were observed before and after every galaxy observation; the primary flux density calibrator was PKS B1934–638.

Standard calibration and data reduction were performed using MIRIAD (Sault *et al.* 1995). Natural weighting was applied to both frequencies to maximise sensitivity. The data were CLEANed and since all fields contained at least one compact object, self-calibration was used to provide additional corrections. Despite limited *uv* coverage using the snapshot method, the noise level in each image was close to theoretical, measuring 70–90 μ Jy beam $^{-1}$ rms. The resolution of the images ranged from 2" to 4" FWHM at 3 cm and 4" to 8" FWHM at 6 cm.

3.2. PTI

Radio interferometry observations were made at 13 cm using the Parkes-Tidbinbilla Interferometer during two sessions in 1996, June 1–2 and October 19–20. Two bandpasses, centred on 2.290 GHz and 2.298 GHz, were observed simultaneously, each with bandwidths of 8 MHz. The data were recorded in real-time using a microwave link between the 64 m Parkes radio telescope and the 70 m telescope at Tidbinbilla (part of the Canberra Deep Space Communication Complex), providing a fringe spacing of 0.1" at 2.3 GHz. Nineteen sample galaxies were observed with PTI as well as three starburst galaxies and three AGNs

for comparison purposes. Unfortunately, it was not possible to observe galaxies with RAs between 16^h–20^h as the Tidbinbilla telescope was being used to track the *Galileo* spacecraft. Each galaxy was observed at a single hour angle for approximately 20 minutes; unresolved flat-spectrum calibrators were observed about every 2 hours.

The AIPS task FRING was used to search for detections in both delay and fringe rate, by applying a Fourier transform fringe-search technique. In this way, we have been able to detect sources that are offset from the phase and delay centre by plotting the correlated intensity as a function of fringe frequency; fringe rate and delay were then used to calculate source positions. Sources were detected up to 3' away from the pointing centre. Furthermore, to ensure that we did not miss any detections of galaxies within the sample due to strong off-centre sources, FRING was run repeatedly, while decreasing the area searched in delay and rate (see Section 4.3).

4. Results

4.1. Radio Imaging

Sixteen galaxies with declinations $< -15^\circ$ (see Table 1) were observed with the ATCA, including four close galaxy pairs (ESO 550-IG025, ESO 440-IG058, ESO 527-IG07 and ESO 343-IG013) and two merging galaxies (MCG-02-33-098 and MCG-02-33-099). Optical spectra of these galaxies, given in the literature, identify them as intermediate between starbursts and AGNs (see Section 2 and Paper 1) with two exceptions: the western nucleus of ESO 527-IG07 has no published optical spectrum, and the merging galaxy MCG-02-33-099 has an optical spectrum typical of a starburst.

In Figure 1 we present the ATCA 6 cm images overlaid as contours on images from the Digitized Sky Survey (DSS), using the second epoch (red-sensitive) DSS-II.³ Of the 14 composite galaxies, 13 were detected with the ATCA and in the majority of cases the emission is unresolved. The only non-detection was the northern nucleus of ESO 440-IG058, which has a 3σ upper limit of

³We note that Deutsch (1999) has found positional errors $\sim 1''$ (≈ 1 pixel) in both RA and Dec for some images in the prepublication release of the DSS-II.

0.2 mJy.

Extended radio structure was found in two galaxies: the southern galaxy in the pair ESO 440-IG58 and the southern galaxy in the pair ESO 343-IG013. The latter pair, in particular, appears to represent a current interaction with tidal tails being seen in optical images. In Figure 2 we present the ATCA 3 cm images overlaid as contours on the DSS-II images for ESO 440-IG058 and ESO 343-IG013. The increased resolution of the 3 cm images shows that the extended radio emission in ESO 440-IG058 south probably traces the star formation in the disk of the galaxy.

Total flux densities for the galaxies, given in Table 2, were obtained using the MIRIAD task SFIND, which performs a Gaussian profile fit. We also include 20 cm flux densities from the NRAO VLA Sky Survey (NVSS) (Condon *et al.* 1998). The NVSS images (45" FWHM) are of lower resolution than the ATCA images so, not surprisingly, the four galaxy pairs observed with the ATCA (ESO 550-IG025, ESO 440-IG058, ESO 527-IG07 and ESO 343-IG013) and the pair of merging galaxies (MCG-02-33-098 and MCG-02-33-099) are detected as single sources by the NVSS. For ESO 440-IG058, ESO 527-IG07 and ESO 343-IG013 the 20 cm emission appears to be centered on the dominant ATCA source. For the non-interacting galaxies the 20 cm emission aligns closely with the ATCA emission, except for ESO 374-IG032 where the NVSS image includes an unrelated source detected at 6 cm with ATCA, lying 45" south of the galaxy. For this galaxy, therefore, and for the galaxy pairs, we have divided the 20 cm flux density into two components in proportion to their 6 cm flux densities.

4.2. Spectral Index

Ideally, to determine the spectral index, α (where $S \propto \nu^\alpha$), of the composite galaxies we require a scaled array in which the baselines (in wavelengths) at 3 and 6 cm are matched. We approximate a scaled array for the 3 and 6 cm images by applying natural weighting to both data sets, thereby giving more significance to the shorter baselines, and by convolving the 3 cm images to the corresponding 6 cm beam so that the images are brought to the same resolution.

Although the spectral index is often determined

between just two frequencies, we draw on the NVSS data to expand the frequency baseline. In Table 2, we present the spectral index for each nucleus, measured between 3–6 cm ($\alpha(6,3)$) and 6–20 cm ($\alpha(20,6)$). Starburst and Seyfert galaxies typically have a spectral index of $\alpha \approx -0.7$, although Seyferts are more likely to have steeper spectra, with $\alpha < -1.1$. (e.g., de Bruyn & Wilson 1978; Sramek & Weedman 1986; Edelson 1987). The mean spectral index for our galaxies, $\alpha(6,3) = -0.65 \pm 0.08$, is consistent with the expected value for both starbursts and Seyferts. The galaxy ESO 436-G026 has an unusually flat spectrum between 3 and 6 cm that steepens significantly towards 20 cm. We attribute this to the presence of a flat-spectrum AGN core, as this galaxy was detected with PTI and has a high core-to-total flux density ratio (see Section 4.3).

4.3. PTI

Unresolved radio emission (referred to here as a PTI ‘core’) was detected in five of the 20 composite galaxies observed with PTI. The sensitivity limit of PTI, corresponding to a 3σ detection, was measured to be 0.9 mJy at 13 cm. The flux densities of the five PTI cores are given in Table 3, as well as the estimated total 13 cm flux densities derived from the data in Table 2. In addition to system noise, the PTI core flux densities have nominal errors of $\approx 7\%$ due to uncertainty in the antenna gains. Studies of radio galaxies involving multiple observations of individual sources (Slee *et al.* 1994; Morganti *et al.* 1997) have shown that the correlated PTI flux density can scatter by as much as 20% due to time variability and/or source structure. In our study only one galaxy, Mrk 1344, was observed twice, in 1996 June and again in 1996 October, and the two measurements agree to well within the combined calibration errors.

We now raise the question: Is our detection rate of 25% consistent with a sample of galaxies that contain AGNs? In the first instance we compare this result with the detection rate found for the three starburst galaxies and three Seyfert galaxies we observed for comparison in this study. PTI cores were detected in two of the three Seyfert galaxies but in none of the starbursts. This result is typical of other studies: Norris *et al.* (2000) detected only one of 74 starburst galaxies but

obtained a PTI detection rate of 38% from 221 Seyferts; Heisler *et al.* (1998) detected none of three starbursts but found PTI cores in 10 out of 11 Seyferts. We propose that the detection rate for our composite sample, while not being exceptionally high, is consistent with a sample of AGNs, assuming that PTI is insensitive to the low brightness temperatures and diffuse structure typical of starbursts. This interpretation is apparently contradicted by studies in which compact radio cores are detected in many starburst galaxies. One such study by Lonsdale *et al.* (1993) found detection rates of eight from 15 starbursts (53%) and seven from 13 Seyferts (54%) with 18 cm VLBI observations. These high detection rates for starburst galaxies, and also Seyferts, are perhaps not surprising as the Lonsdale *et al.* sample was preferentially selected from galaxies known to contain compact radio cores with angular size $\leq 0.25''$. The sample may also be subject to a luminosity selection effect, as it was selected from among the most luminous members of the IRAS Bright Galaxy Sample, with $\log(L_{FIR}/L_\odot) \geq 11.25$.

The detection of VLBI cores in many of the starburst galaxies in the Lonsdale *et al.* (1993) sample, combined with their strong IRAS emission, may simply indicate a dominance of dust-obscured AGNs and does not necessarily imply a starburst origin for the compact cores. The alternative possibility, that a starburst-related process may produce compact radio emission, comes from the discovery of a new class of exceptionally luminous RSNe (Yin & Heeschen 1991; Lonsdale *et al.* 1992; Wilkinson & de Bruyn 1990). Smith *et al.* (1998a) claim that from 11 detections of starburst galaxies, 7 may be explained by extremely luminous RSNe. However, the only galaxy to date where the compact core can definitively be attributed to a starburst is the ultraluminous IRAS galaxy (ULIRG), Arp 220, where high resolution images have revealed numerous unresolved sources interpreted as RSNe (Smith *et al.* 1998b).

To investigate the possibility of RSNe in our sample we follow Smith *et al.* (1998b) and compare our PTI detections with the well studied and unusually bright RSN, SN 1986J in the galaxy NGC 891 (Weiler, Panagia & Sramek 1990). During 1986, SN 1986J peaked at 6 cm reaching a flux density of ~ 130 mJy. Using the (optically thick) spectral index calculated at that time from 6 cm

and 20 cm observations of the supernova, we derive a corresponding 13 cm flux density of ~ 100 mJy. Our sample galaxies are on average 10 times more distant than NGC 891, so if a RSNe similar to 1986J existed in our sample, it would be at a level of approximately 1 mJy and just marginally detectable with PTI. Since 1986J is amongst the most luminous RSNe ever discovered, the nature of the PTI detections is not yet determined.

An interesting caveat in the debate over a starburst or AGN origin of compact radio cores is given in the recent work of Kewley *et al.* (2000a). In their study of warm infrared galaxies, they detected compact radio cores in 8 from 10 (80%) AGNs and 10 from 27 (37%) starbursts. However, the core luminosities of the starburst galaxies were lower than those in the AGNs, suggesting that the starburst cores may be radio-luminous supernovae. Comparing the luminosity of our five PTI detections with those in the Kewley *et al.* sample, we find that three galaxies (ESO 550-IG025, MCG+00-29-23 and IRAS 12224-0624) are consistent with AGN-like compact cores, while the remaining two galaxies (ESO 436-G026 and Mrk 1344) are possibly starburst-related. However, in the specific case of ESO 436-G026, the flatness of its radio spectrum between 3–6 cm does favour the presence of an AGN core.

We cannot tell from the radio data alone whether our PTI detections are weak AGN cores or radio-luminous supernovae. However, we can compare the flux density of the compact core (derived from the PTI detections or 0.9 mJy limits for non-detections) with the total 13 cm flux density (derived from the ATCA observations). These are used to determine a core-to-total flux density ratio, given in Table 3. For the composite galaxies we find on average that a compact core accounts for $< 10\%$ of the total radio emission. Interestingly, the compact radio cores in the reference Seyfert galaxies in Table 3 *also* contribute typically $< 10\%$ of the total. We show in Section 4.7 that a similar AGN contribution in the optical is sufficient to account for the ambiguous optical emission line ratios of the composite galaxies.

4.4. Supernova or AGN

The PTI results indicate that most galaxies in our sample are not AGN-dominated. Since it is generally assumed that the radio emission from

galaxies with starburst characteristics is predominantly non-thermal emission from cosmic rays accelerated by supernova remnants (SNRs), we follow Condon & Yin (1990) and estimate the Type II supernova rate from

$$N_{\text{SN}}(\text{yr}^{-1}) = 7.7 \times 10^{-24} \nu^\alpha L_{\text{NT}}, \quad (1)$$

where L_{NT} is the non-thermal component of the radio luminosity in WHz^{-1} , ν is the frequency in GHz and α is the non-thermal radio spectral index, taken here to be ~ -0.8 . The supernova rate can then be used to estimate the number of ionising photons

$$N_{\text{UV}}(\text{s}^{-1}) = 8.2 \times 10^{54} N_{\text{SN}}(\text{yr}^{-1}) \quad (2)$$

and, by assuming the average ionising flux from OB stars to be $N_{\text{UV}} = 2 \times 10^{48} \text{s}^{-1}$ (Smith, Herter & Haynes 1998), a star-formation rate (SFR) can be derived and is given in Table 4.

Since the SFR is derived from the supernova rate, it is an indication of the past SFR for massive stars in the galaxy, as the progenitors of Type II SNe are massive stars ($M > 8M_\odot$) with lifetimes $\sim 10^6$ years. The SFR may be somewhat over-estimated since we have assumed that all of the radio emission is non-thermal. The empirical relationship between the non-thermal and thermal radio emission (Condon & Yin 1990) suggests that 25% of the total 4.85 GHz radio flux density may be thermal (Smith, Herter & Haynes 1998).

The galaxy NGC 1614 has an inferred supernova rate four times larger than any other galaxy in the sample. It has a high FIR luminosity, and is usually classified as a starburst galaxy (Keto *et al.* 1992). However, based on our selection criteria, NGC 1614 has ambiguous optical emission-line ratios (Veilleux *et al.* 1995). Although Neff *et al.* (1990) find no direct evidence of an AGN in NGC 1614 they suggest that the galaxy may be a precursor to a Seyfert (i.e., the AGN has not yet turned on) due to the high luminosity they measure for the nucleus of the galaxy. No signs of an AGN have been found in other studies of NGC 1614 (Lançon *et al.* 1996; Heisler *et al.* 1999).

The median supernova rate from Table 4 is 0.2 yr^{-1} , which is high compared with the rate of 0.03 yr^{-1} found for Seyfert 2 galaxies with circumnuclear star formation (Forbes & Norris

1998). This suggests a dominance of star formation within our sample. However, it is surprising that Mrk 52, which was found to be dominated by star formation in Paper 1, has an exceptionally weak SFR.

4.5. FIR spectral energy distribution

The heating mechanisms at work in galaxies can be investigated using FIR colours. The majority of IRAS galaxies (70–80%) appear to be dominated by star formation, with the FIR emission being due to dust heating from an intense starburst (Sanders & Mirabel 1996; Leech *et al.* 1989). This appears to hold even for the ULIRGs with $L_{\text{FIR}} > 10^{12} L_\odot$ (Genzel *et al.* 1998). Mergers are also common, with $\approx 70\%$ of the ULIRGs involved in interactions (Leech *et al.* 1994). However, the proportion of mergers does drop considerably for $L_{\text{FIR}} < 10^{11} L_\odot$ (Sanders & Mirabel 1996). The extreme luminosities of some IRAS galaxies, their extensive star formation, and the large fraction of mergers have led to suggestions that these galaxies are presently in a transient phase which may be important in the formation of an active nucleus (Sanders *et al.* 1988).

All the composite galaxies in our sample have published IRAS flux densities and in Figure 3 we present three FIR colour-colour diagrams which can be used to discriminate between starburst and Seyfert excitation. Included in these diagrams are a reddening line, extreme mixing curve and empirical starburst line taken from Dopita *et al.* (1998). The reddening line was obtained by applying IR extinctions given by Dwek *et al.* (1997) to an average Seyfert 1, with flux density normalised to 10 mJy at 100 μm . The empirical starburst line joins the average flux values of a “cool” starburst to a “hot” starburst taken from the data of Rush *et al.* (1993), again with the flux density normalised to 10 mJy at 100 μm . The extreme mixing line was determined by adding a percentage of the “cool” starburst flux to the non-reddened average Seyfert 1 value. Dopita *et al.* (1998) make it clear that any number of mixing curves can be added to these FIR colour-colour diagrams but the mixing curve used here is an extreme solution and, therefore, all objects are expected to lie within the region bounded by the reddening line, the empirical starburst line and the extreme mixing curve.

In Figure 3a the composite galaxies lie along

the starburst line, while in Figures 3b and 3c the composite galaxies are clustered around the top end of the AGN/starburst mixing curve. This indicates that star formation is dominating the FIR emission, with a starburst contribution of $> 90\%$, consistent with the PTI results which place the AGN contribution at $< 10\%$.

4.6. FIR-radio correlation

One of the tightest correlations for radio-quiet star-forming galaxies is found between the FIR and radio luminosities. Although the correlation has been known for two decades or more (Dickey & Salpeter 1984; de Jong *et al.* 1985; Wunderlich, Klein & Wielebinski 1987; Condon 1992), its origin is still not clear. Starburst activity is one likely explanation: the massive OB stars formed within starbursts heat the surrounding dust which re-radiates in the FIR, while the radio emission comes about through the death of these massive stars as supernovae that accelerate cosmic rays and in turn produce synchrotron radiation (Helou & Bicay 1993; Volk 1989). The uncertainty in this scenario is in the feedback mechanism required to link the FIR and radio emission so tightly.

Starburst galaxies generally show a tighter FIR-radio correlation than Seyferts (Roy *et al.* 1998; Condon 1992; Norris *et al.* 1988a), while the more energetic AGNs, such as quasars and radio galaxies, do not fit the correlation due to enhanced radio emission from the AGN (Sopp & Alexander 1991). The FIR-radio correlation for the present sample is shown in Figure 4, together with the fit from de Jong *et al.* (1985). The composite galaxies are also seen to follow the correlation. If the starburst origin for this correlation is correct, then star formation is again seen to be the dominant process in these galaxies.

4.7. Comparison with optical and NIR spectroscopy

As mentioned in Section 2, the sample of composite galaxies was chosen on the basis of the Veilleux & Osterbrock (1987) optical emission-line diagnostic diagrams. These diagrams are presented in Figure 5 and include starburst and AGN data from the literature, and also two photoionisation models developed in Paper 1 using MAPINGS II (see Sutherland & Dopita 1993). The

starburst model is based on the stellar atmosphere models of Hummer & Mihalas (1970) with a stellar temperature of 40 000 K, while the AGN model was created from a power-law ionising spectrum of the form $f_\nu \sim \nu^\alpha$, with $\alpha = -1.5$. Other model parameters include a hydrogen density of 10^3 cm^{-3} and solar metallicity.

The galaxies that were detected with PTI do not appear to occupy any special position within Figure 5. However, we have also included on the diagnostic diagrams a mixing line from the low-ionisation starburst galaxies to the high-ionisation AGNs. The end points for the mixing line were determined by taking a median of the emission-line ratios for starbursts and AGNs (with a cut-off of $\log([\text{OIII}]/\text{H}\alpha) > 0.5$ applied to the AGN ratios to omit LINERS) taken from Veilleux & Osterbrock (1987 and references therein) and Veilleux *et al.* (1995). It becomes evident that an AGN contribution of $\approx 10\%$ of the total emission of the galaxy can still account for the borderline position of the composite galaxies within the diagnostic diagrams. In fact, it has been recently found that the optical diagnostic diagrams are especially sensitive to the presence of an AGN. Kewley *et al.* (2000b) applied a mixing line from their photoionisation (or starburst) model to their shock (or AGN) model and found that objects with as little as 20% AGN contribution to their energy budget may be classified as AGN in the optical diagnostic diagrams.

Our study of NIR diagnostic diagrams in Paper 1 found that the line ratio diagram of $[\text{Fe II}]/\text{Pa}\beta$ vs $[\text{O I}]/\text{H}\alpha$ was the most useful for distinguishing starbursts and Seyferts. This diagram is shown in Figure 6 with the same starburst and power-law models presented in Figure 5 and with the composite galaxies again differentiated by the PTI detections. The two galaxies detected with PTI, and for which we have NIR data, have the largest $[\text{Fe II}](1.25\mu\text{m})/\text{Pa}\beta$ ratios and therefore are most likely to be classified as AGNs from this diagram (see Paper 1).

5. Conclusions

We have presented arc-second radio images and long-baseline radio interferometer observations to extend our study of composite galaxies with ambiguous optical emission-line ratios. Extended ra-

dio morphology in radio-quiet galaxies is usually attributed to starbursts and we found that only two galaxies, ESO 440-IG058 south and ESO 343-IG013 south, showed extended emission with the ATCA. The radio continuum images were also used to derive spectral indices for the galaxies, with the average being $\alpha(6,3) = -0.65 \pm 0.08$ which is typical of both starbursts and Seyferts.

Our interferometry observations revealed compact cores in five of the 20 galaxies observed, which may be due either to a weak (< 10% of total flux density) AGN component or a radio-luminous supernova. The majority of non-detections for the sample does not rule out the existence of an AGN core but points to the starburst being the dominant flux density contribution within the galaxies. A similar result was found upon examining the FIR emission which we also found to be dominated by star formation.

From our radio observations and examination of the FIR fluxes we conclude that star formation dominates the composite galaxies, and we attribute only a small fraction of the emission ($\leq 10\%$) to an AGN component. However, we have shown that an AGN contribution as small as this is still sufficient to identify the galaxies as composites within the optical diagnostic diagrams.

We thank Edward King and staff at the Tidbinbilla Tracking Station for help with the PTI observations. We also thank the referee for insightful comments which greatly improved this paper. TLH acknowledges receipt of an Australian Postgraduate Award, and thanks Museum Victoria and Rachel Webster for support during the writing of this paper. RWH acknowledges funding from the Australian Research Council. The Australia Telescope Compact Array and the Parkes Telescope are part of the Australia Telescope which is funded by the Commonwealth of Australia for operation as a National Facility managed by CSIRO. This research has made use of the NASA Astrophysics Data System service and of the NASA/IPAC Extragalactic Database which is operated by the Jet Propulsion Laboratory, California Institute of Technology, under contract with the National Aeronautics and Space Administration. This research has also made use of the Digitized Sky Surveys (DSS) produced at the Space Telescope Science Institute under U.S. Government

grant NAG W-2166.

REFERENCES

Ashby, M. L. N., Houck, J. R. & Matthews, K. 1995, *ApJ*, 447, 545.

Burgess, A. M. & Hunstead R. W. 1995 *PubASA*, 12, 227.

Condon, J. J. 1992, *ARA&A*, 30, 575.

Condon, J. J., Cotton, W. D., Greisen, E. W., Yin, Q. F., Perley, R. A., Taylor, G. B. & Broderick, J. J. 1998, *AJ*, 115, 1693.

Condon, J. J. & Yin, Q. F. 1990, *ApJ*, 357, 97.

Crawford, T., Marr, J., Partridge, B., & Strauss, M. A. 1996, *ApJ*, 460, 225.

de Bruyn, A. G. & Wilson, A. S., 1978 *A&A*, 64, 433.

de Jong, T., Klein, U., Wielebinski, R., and Wunderlich, E. 1985 *A&A*, 147, L6.

Deutsch, E. W. 1999, *AJ*, 118, 1882.

Dickey, J. M., & Salpeter, E. E. 1984, *ApJ*, 284, 461.

Dopita, M. A., Heisler, C. A., Lumsden, S., & Bailey, J. 1998, *ApJ*, 498, 570.

Dwek, E., Arendt, R. G., Fixsen, D. J., Sodroski, T. J., Odegard, N., Weiland, J. L., Reach, W. T., Hauser, M. G., Kelsall, T., Moseley, S. H., Silverberg, R. F., Shafer, R. A., Ballester, J., Bazell, D. & Isaacman, R. 1997, *ApJ*, 475, 565.

Edelson, R. A. 1987, *ApJ*, 313, 651.

Forbes, D. A. and Norris, R. P. 1998, 300, 757.

Gallimore, J. F., Baum, S. A., & O'Dea, C. P. 1997, *Nature* 388, 852.

Genzel, R., Lutz, D., Sturm, E., Egami, E., Kunze, D., Moorwood, A.F.M., Rigopoulou, D., Spoon, H. W. W., Sternberg, A., Tacconi-Garman, L. E., Tacconi, L. & Thatte, N., 1998, *ApJ*, 498, 579.

Genzel, R., Weitzel, L., Tacconi-Garman, L. E., Blietz, M., Cameron, M., Krabbe, A., Lutz, D. & Sternberg, A. 1995, *ApJ*, 444, 129.

Heckman, T. M., Gonzalez-Delgado, R., Leitherer, C., Meurer, G. R., Krolik, J., Wilson, A. S., Koratkar, A. & Kinney, A. 1997, *ApJ*, 482, 114.

Heisler, C. A., Dopita, M. A., Kewley, L. and Lumsden, S., 1999, Ringberg Workshop on Ultraluminous Galaxies, in press.

Heisler, C. A., Norris, R. P., Jauncey, D. L., Reynolds, J. E. & King, E. A., 1998, *MNRAS*, 300, 757.

Helou, G. & Bicay, M. D. 1993, *ApJ*, 415, 93.

Hill, T. L., Heisler, C. A., Sutherland R. & Hunstead, R. W. 1999, *AJ*, 117, 111 (Paper 1).

Hummer, D. G., & Mihalas, D. M. 1970, *MNRAS*, 147, 339.

Keto, E., Ball, R., Arens, J., Jernigan, G. and Meixner, M. 1992 *ApJ*, 389, 223.

Kewley, L., Heisler, C., Dopita, M. & Norris, R. 2000a *ApJ*, 530, 704.

Kewley, L. J., Heisler, C. A., Dopita, M. A. & Lumsden, S. 2000b *ApJS*, submitted.

Lançon, A. & Rocca-Volmerange, B. 1996, *New Astronomy*, 1, 215.

Leech, K. J., Penston, M. V., Terlevich, R. J., Lawrence, A., Rowan-Robinson, M. & Crawford, J., 1989, *MNRAS*, 240, 349.

Leech, K. J., Rowan-Robinson, M., Lawrence, A. & Hughes, J. D., 1994, *MNRAS*, 267, 253.

Lonsdale, C. J., Lonsdale, C. J., & Smith, H. E. 1992, *ApJ*, 391, 629.

Lonsdale, C. J., Smith, H. E., & Lonsdale, C. J. 1993, *ApJ*, 405, L9.

Morganti, R., Oosterloo, T. A., Reynolds, J. E., Tadhunter, C. N. & Migenes, V., 1997, *MNRAS*, 284, 541.

Mouri, H., Kawara, K. & Taniguchi, Y. 1993, *ApJ* 406, 52.

Mouri, H., Nishida, M., Taniguchi, Y., & Kawara, K. 1990, *ApJ*, 360, 55.

Neff, S. G., Hutchings, J. B., Stanford, S. A. and Unger S. W. 1990, *AJ*, 99, 1088.

Norris, R. P., Allen, D. A. & Roche, P. F. 1988a, *MNRAS*, 234, 773.

Norris, R. P., Heisler, C. A. & Roy, A. L. 2000, in preparation.

Norris, R. P., Kesteven, M. J., Wellington, K. J. & Batty, M. J. 1988b, *ApJS*, 67, 85.

Oliva, E., Origlia, L., Kotilainen, J. K., & Moorwood, A. F. M. 1995, *A&A*, 301, 55.

Roy, A. L., Norris, R. P., Kesteven, M. J., Troup, E. R. and Reynolds, J. E. 1998, *MNRAS*, 301, 1019.

Rush, B., Malkan, M. A., & Spinoglio, L. 1993, *ApJS*, 89, 1.

Sault, R. J., Tueben, P. J., & Wright, M. C. H. 1995, in *Astronomical Data Analysis Software and Systems IV*, eds. R. Shaw, H. E. Payne, J. J. E. Hayes, *ASP Conf. Ser.* 77, 433.

Sanders, D. B. & Mirabel, I. F., 1996, *ARA&A*, 34, 749.

Sanders, D. B., Soifer, B. T., Elias, J. H., Madore, B. F., Matthews, K., Neugebauer, G. & Scoville, N. Z., *ApJ*, 1988, 325, 74.

Simpson, C., Forbes, D. A., Baker, A. C. & Ward, M. J. 1996, *MNRAS*, 283, 777.

Slee, O. B., Sadler, E. M., Reynolds, J. E., & Ekers, R. D. 1994, *MNRAS*, 269, 928.

Smith, D. A., Herter, T., & Haynes, M. P. 1998, *ApJ*, 494, 150.

Smith, H. E., Lonsdale, C. J. & Lonsdale, C. J. 1998a, *ApJ*, 492, 137.

Smith, H. E., Lonsdale, C. J., Lonsdale, C. J. & Diamond, P. D. 1998b, *ApJ*, 493, L17.

Sopp, H. M., & Alexander, P. 1991, *MNRAS*, 251, 14p.

Sramek, R. A. & Weedman, D. W., 1986, *ApJ*, 302, 640.

Sutherland, R. S. & Dopita, M. A. 1993, *ApJS*, 88, 253.

Thatte, N., Quirrenbach, A., Genzel, R., Maiolino, R., and Tecza, M. 1997, *ApJ*, 490, 238.

van den Broek, A. C., van Driel, W., de Jong, T., Lub, J., de Grijp, M. H. K., & Goudfrooij, P. 1991, *A&AS*, 91, 61.

Veilleux, S., Kim, D. -C., Sanders, D. B., Mazzarella, J. M. & Soifer, B. T. 1995, *ApJS*, 98, 171.

Veilleux, S. & Osterbrock, D. E. 1987, *ApJS*, 63, 295.

Volk, H. J., 1989, *A&A*, 218, 67.

Weiler, K. W., Panagia, N. & Sramek, R. A. 1990, *ApJ*, 364, 611.

Wilkinson, P. N. & de Bruyn, A. G. 1990, *MNRAS*, 242, 529.

Wilson, A. S. 1988, *A&A*, 206, 41.

Wilson, A., Helfer, T., Haniff, C., & Ward, M. 1991, *ApJ*, 381, 79.

Wilson, A. S. & Ulvestad, J. S. 1982, *ApJ*, 263, 576.

Wunderlich, E., Wielebinski, R., Klein, U. 1987, *A&AS*, 69, 487.

Wynn-Williams, C. G., Becklin, E. E., & Scoville, N. Z., 1985, *ApJ*, 297, 607.

Yin, Q. F. & Heeschen, D. S. 1991, *Nature*, 354, 130.

TABLE 1
OBSERVING LOG

Galaxy	Optical position		z	ATCA	PTI
	RA(J2000)	Dec(J2000)		Int. Time (min)	Obs
NGC 232	00 42 45.9	-23 33 36	0.023	228	Y
NGC 1204	03 04 40.4	-12 20 28	0.015	...	Y
ESO 550-IG025 N	04 21 19.9	-18 48 39	0.032	139	Y
ESO 550-IG025 S	04 21 20.0	-18 48 56	0.032	139	Y
NGC 1614	04 33 59.8	-08 34 44	0.016	...	Y
ESO 374-IG032	10 06 04.5	-33 53 08	0.034	108	Y
IRAS 10057-3343	10 07 59.1	-33 58 07	0.034	98	Y
ESO 500-G034	10 24 31.4	-23 33 11	0.013	101	Y
ESO 436-G026	10 28 42.7	-31 02 18	0.014	130	Y
MCG+00-29-23	11 21 11.7	-02 59 03	0.025	...	N
Mrk 739 (NGC 3758)	11 36 29.1	+21 35 48	0.030	...	Y
ESO 440-IG058 N	12 06 51.7	-31 56 47	0.023	167	Y
ESO 440-IG058 S	12 06 51.8	-31 56 58	0.023	167	Y
IRAS 12224-0624	12 25 04.0	-06 40 53	0.026	...	Y
Mrk 52 (NGC 4385)	12 25 42.6	+00 34 23	0.0071	...	Y
MCG-02-33-098 ^a	13 02 19.9	-15 46 06	0.017	175	Y
Mrk 1344 (NGC 4990)	13 09 17.2	-05 16 23	0.011	...	Y
NGC 5713 N ^b	14 40 11.1	-00 17 02	0.0073	...	Y
NGC 5719	14 40 56.7	-00 18 58	0.0058	...	Y
NGC 5937	15 30 46.6	-02 49 32	0.0094	...	Y
ESO 527-IG07 E ^c	20 04 31.3	-26 25 40	0.035	175	N
ESO 343-IG013 N	21 36 11.1	-38 32 33	0.019	197	Y
ESO 343-IG013 S	21 36 11.0	-38 32 42	0.019	197	Y
ESO 602-G025	22 31 25.3	-19 02 05	0.025	208	Y
Starbursts					
AKN 232	10 07 38.8	+17 06 02	0.026	...	Y
Mrk 717 (IC 2551)	10 10 40.3	+24 24 51	0.021	...	Y
Mrk 529 (NGC 7532)	23 14 22.2	-02 43 39	0.010	...	Y
Seyferts					
Mrk 955	00 37 35.8	+00 16 51	0.035	...	Y
NGC 3627 (M66)	11 20 15.0	+12 59 30	0.0024	...	Y
NGC 4569 (M90)	12 36 49.8	+13 09 46	0.00078	...	Y

^aMCG-02-33-098 is the western galaxy of an interacting pair. The eastern galaxy, MCG-02-33-099 has an optical spectrum typical of a starburst.

^bThe southern nucleus of NGC 5713 has an optical spectrum typical of a starburst.

^cThe western nucleus of ESO 527-IG07 has no published optical spectrum.

TABLE 2
RADIO CONTINUUM FLUX DENSITIES & SPECTRAL INDICES

Galaxy	Radio position		3 cm ^a	6 cm	20 cm ^b	$\alpha(6,3)$	$\alpha(20,6)$
	RA(J2000)	Dec(J2000)	(mJy)	(mJy)	(mJy)		
NGC 232	00 42 45.8	-23 33 41	14.3	22.4	60.6	-0.76	-0.81
NGC 1204	03 04 40.0	-12 20 30	26.4
ESO 550-IG025 N	04 21 20.0	-18 48 39	7.2	10.5	28.3 ^c	-0.64	-0.80
ESO 550-IG025 S	04 21 20.0	-18 48 57	3.2	5.2	13.3 ^c	-0.83	-0.76
NGC 1614	04 34 00.0	-08 34 45	...	63 ^d	138.2	...	-0.64
ESO 374-IG032	10 06 04.6	-33 53 06	3.7	5.5	18.7 ^c	-0.67	-0.99
IRAS 10057-3343	10 07 59.0	-33 58 06	3.7	5.3	13.2	-0.61	-0.74
ESO 500-G034	10 24 31.5	-23 33 11	15.7	22.0	57.8	-0.57	-0.78
ESO 436-G026	10 28 42.9	-31 02 17	2.9	3.0	11.9	-0.01	-1.12
Mrk 739	11 36 29.2	+21 35 49	11.2
ESO 440-IG058 N	<0.3 ^e	<0.2 ^e
ESO 440-IG058 S	12 06 51.9	-31 56 59	9.7	18.4	52.1	-1.09	-0.84
IRAS 12224-0624	12 25 04.1	-06 40 54	11.2
Mrk 52	12 25 42.8	+00 34 23	14.8
MCG-02-33-098	13 02 19.7	-15 46 04	5.6	7.7	22.1 ^c	-0.54	-0.86
Mrk 1344	13 09 17.3	-05 16 21	29.9
NGC 5713	14 40 11.3	-00 17 26	...	81 ^d	159.9	...	-0.55
NGC 5719	14 40 56.3	-00 19 07	58.7
NGC 5937	15 30 46.1	-02 49 47	114.0
ESO 527-IG07 E	20 04 31.0	-26 25 39	4.0	6.1	12.8 ^c	-0.72	-0.60
ESO 343-IG013 N	21 36 10.9	-38 32 33	2.6	3.2	7.9 ^c	-0.35	-0.73
ESO 343-IG013 S	21 36 10.6	-38 32 43	5.6	7.8	18.0 ^c	-0.56	-0.68
ESO 602-G025	22 31 25.5	-19 02 04	7.4	14.2	46.5	-1.11	-0.96
Starbursts							
AKN 232	10 07 38.8	+17 06 02
Mrk 717 (IC 2551)	10 10 40.3	+24 24 50	26.0
Mrk 529 (NGC 7532)	23 14 22.3	-02 43 42	11.6
Seyferts							
Mrk 955	00 37 36.0	+00 16 53	8.4
NGC 3627 (M66)	11 20 16.8	+12 58 46	...	141 ^f	466 ^g
NGC 4569 (M90)	12 36 49.6	+13 09 57	73.1

^aThe 3 cm image has been convolved to the 6 cm beamwidth to approximate a scaled array.

^bThe 20 cm flux densities are taken from the NVSS (Condon *et al.* 1998)

^cThe NVSS source is blended, and the 6 cm ATCA flux densities have been used to determine the relative contributions at 20 cm.

^dGriffith *et al.* (1995)

^e3 σ limit

^fGregory *et al.* (1995)

^gThis is a complicated region where three NVSS sources are blended.

TABLE 3
PTI DETECTIONS AND UPPER LIMITS

Galaxy	Position of PTI detection		PTI flux	Total 13 cm	core/
	RA(J2000)	Dec(J2000)	density (mJy)	flux density ^a (mJy)	total
NGC 232	<0.9	39.2	<2%
NGC 1204	<0.9	19.6	<5%
ESO 550-IG025	04 21 18.3	-18 48 49	1.9	26.2	7%
NGC 1614	<0.9	102	<0.9%
ESO 374-IG032	<0.9	9.1	<10%
IRAS 10057-3343	<0.9	8.1	<11%
ESO 500-G034	<0.9	33.5	<3%
ESO 436-G026	10 28 43.3	-31 02 22	1.0	3.0	33%
MCG+00-29-23	5 ^b
Mrk 739	<0.9	8.3	<11%
ESO 440-IG058	<0.9	41.3	<2%
IRAS 12224-0624	12 25 05.9	-06 40 29	3.1	8.3	37%
Mrk 52	<0.9	11.0	<8%
MCG-02-33-098	<0.9	11.5	<8%
Mrk 1344	13 09 17.3	-05 16 21	3.5	22.2	16%
NGC 5713 N	<0.9	119	<0.8%
NGC 5719	<0.9	43.5	<2%
NGC 5937	<0.9	84.5	<1%
ESO 343-IG013	<0.9	15.9	<6%
ESO 602-G025	<0.9	31.9	<3%
Starbursts					
AKN 232	<0.9
Mrk 717	<0.9	19.2	<5%
Mrk 529	<0.9	8.6	<10%
Seyferts					
Mrk 955	<0.9	6.2	<15%
NGC 3627	11 20 15.5	+12 59 20	2.0	345	0.6%
NGC 4569	12 36 46.6	+13 09 12	1.1	54.2	2%

^aDerived from 6 cm flux density and $\alpha(6,3)$ spectral index; however, if no ATCA data was available we used the 20 cm fluxes and assumed a spectral index of -0.7.

^bNorris *et al.* (1990)

TABLE 4
DERIVED SUPERNOVA AND STAR FORMATION RATES

Galaxy	N_{SN} yr^{-1}	SFR($M > 8M_{\odot}$) $M_{\odot} yr^{-1}$
NGC 232	0.62	3.1
NGC 1204	0.12	0.6
ESO 550-IG025	0.88	4.4
NGC 1614	3.39	16.9
ESO 374-IG032	0.33	1.7
IRAS 10057-3343	0.32	1.6
ESO 500-G034	0.19	1.0
ESO 436-G026	0.03	0.2
MCG+00-29-023
Mrk 739	0.20	1.0
ESO 440-IG058	0.51	2.5
IRAS 12224-0624	0.15	0.8
Mrk 52	0.01	0.07
MCG-02-33-098	0.19	0.9
Mrk 1344	0.07	0.4
NGC 5713	0.21	1.0
NGC 5719	0.59	0.3
NGC 5937	0.19	0.9
ESO 527-IG07 E	0.61	3.1
ESO 343-IG013	0.22	1.1
ESO 602-G025	0.46	2.3

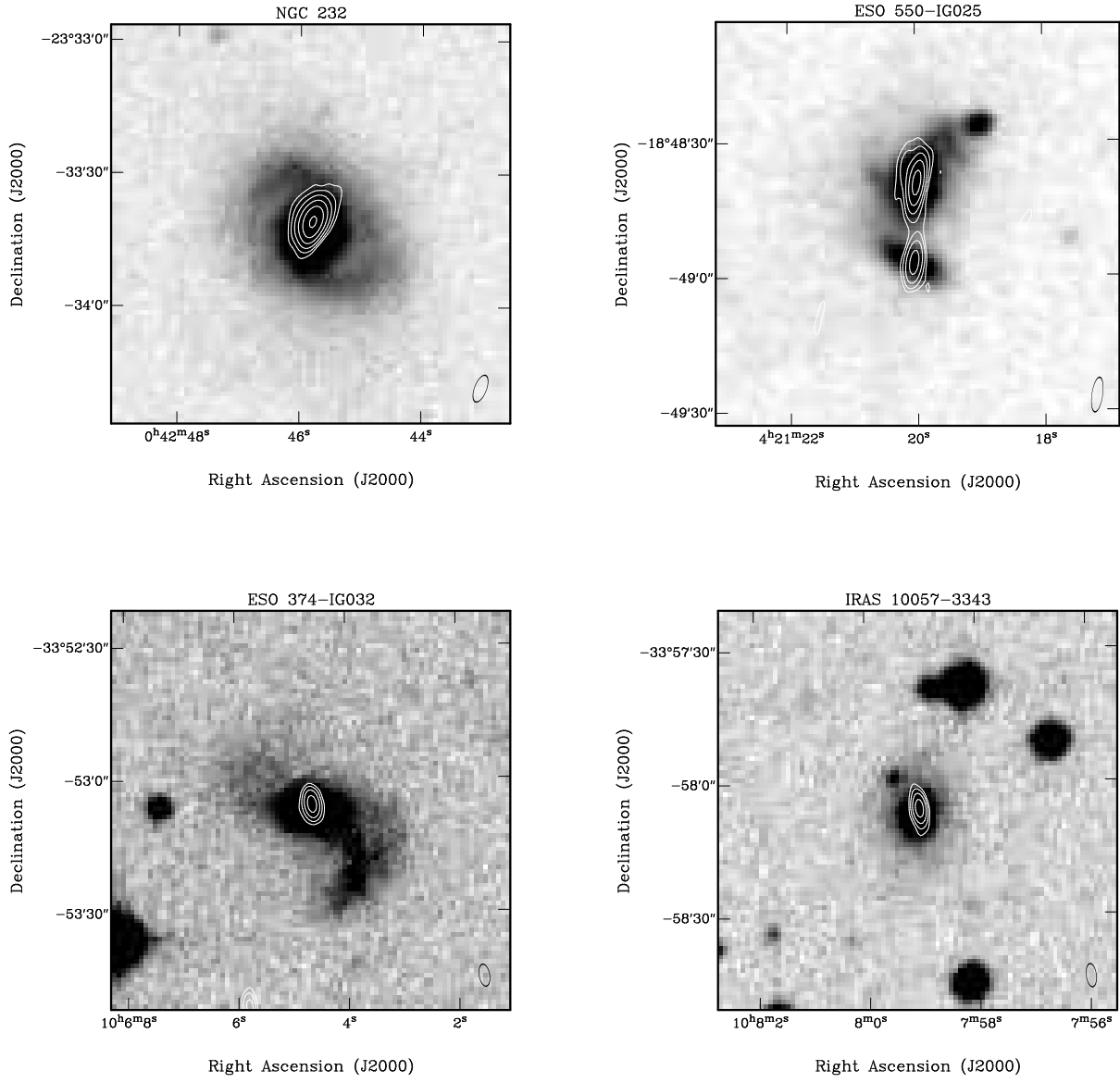


Fig. 1.— DSS images (greyscale) overlaid with 6 cm ATCA images (contours) for all the composite galaxies. The contours are at 0.4, 0.8, 1.6, 3.2, 6.4 and 12.8 mJy beam $^{-1}$. The synthesised half-power beam-shape is shown as an ellipse in the lower right corner of each image. The red-sensitive DSS-II has been used for all overlays except MCG-02-33-098 which uses the blue DSS-I.

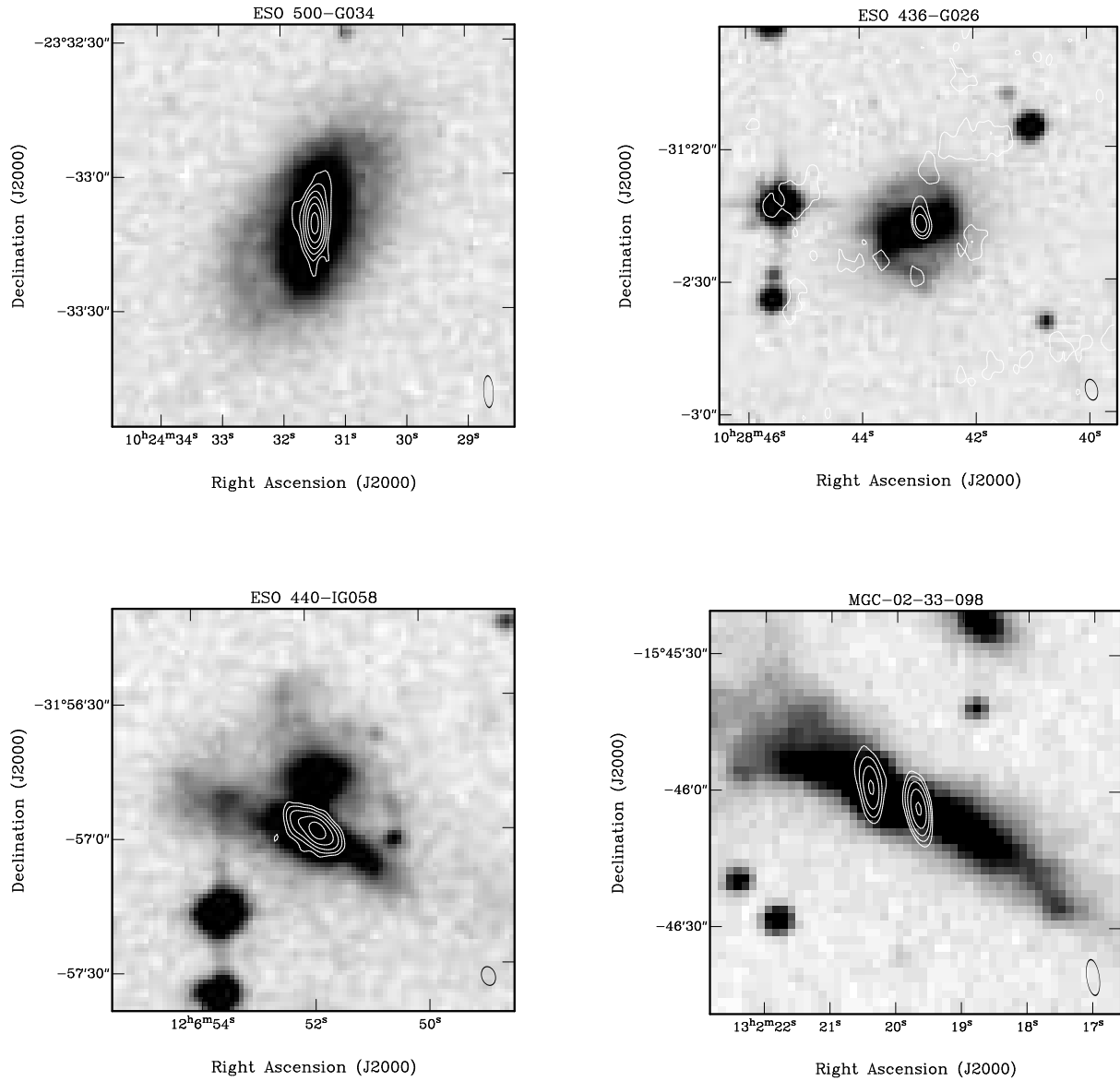


Fig. 1.— *cont.*

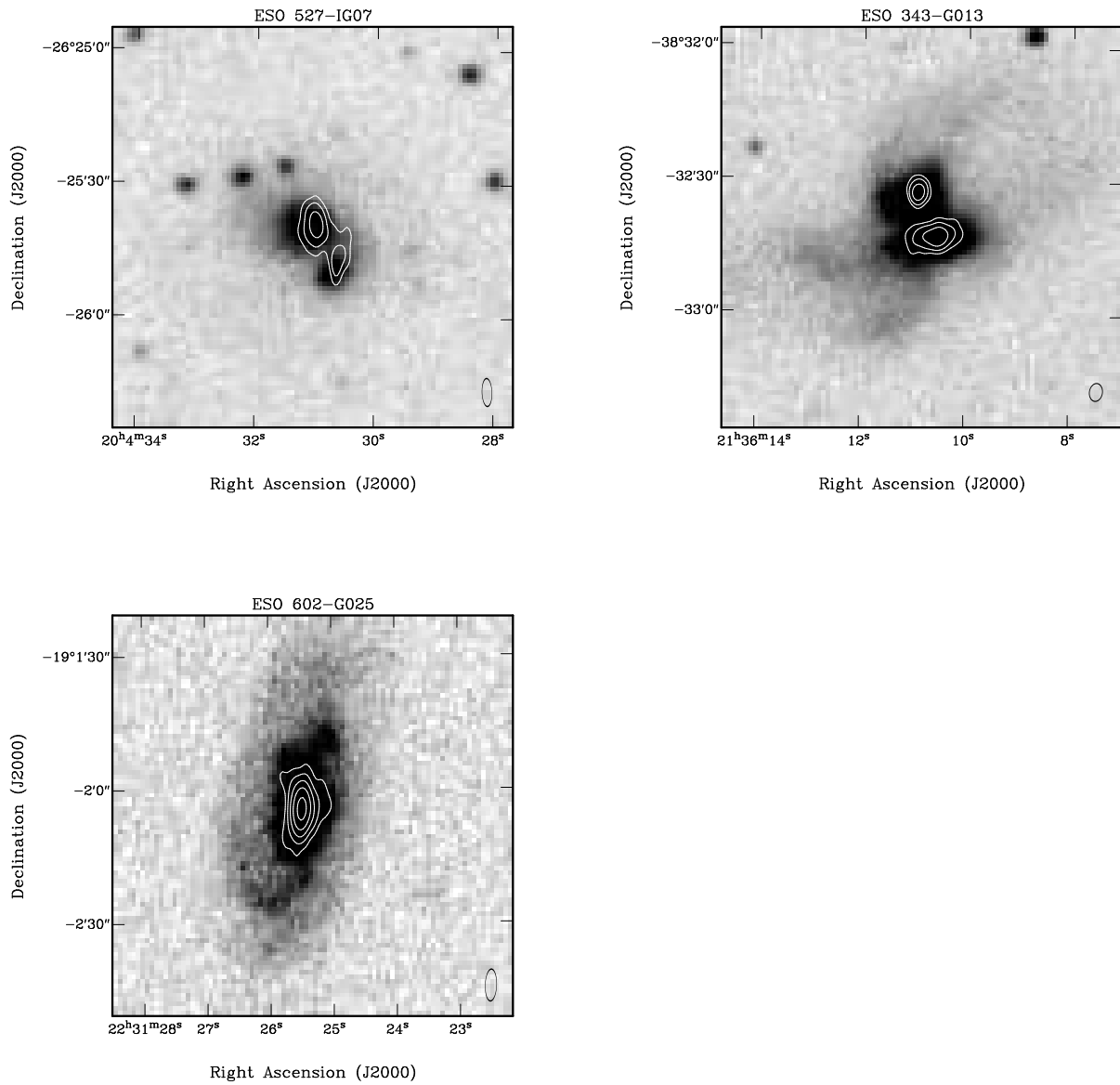


Fig. 1.— *cont.*

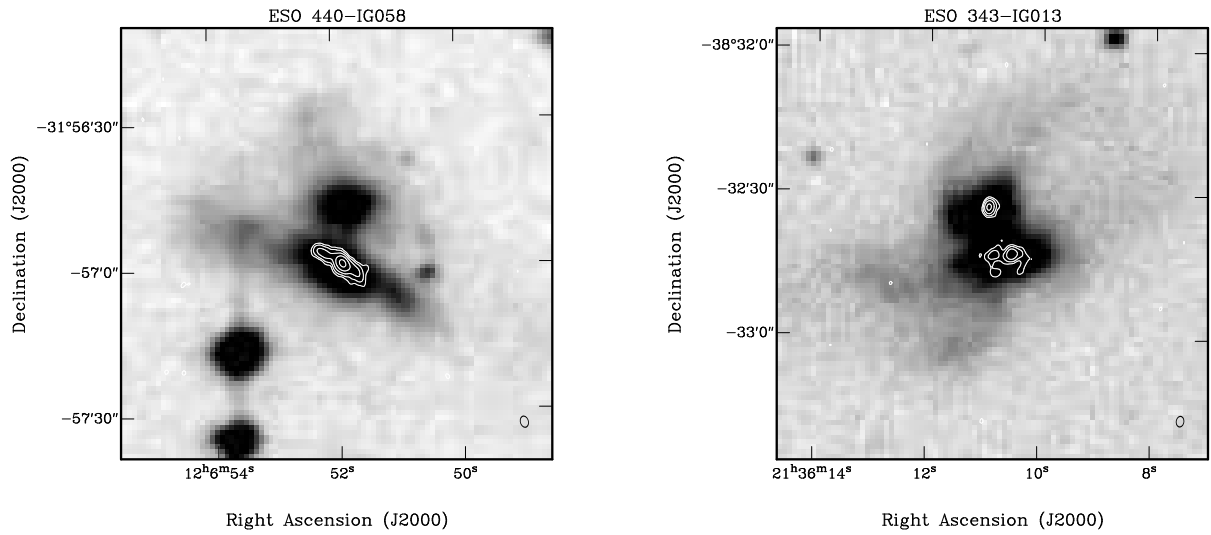


Fig. 2.— DSS-II images (greyscale) overlaid with 3 cm ATCA images (contours) for the two galaxies in the sample with extended emission. The contours are at 0.2, 0.4, 0.8, 1.6, 3.2 mJy beam $^{-1}$. The synthesised half-power beam-shape is shown as an ellipse in the lower right corner of each image.

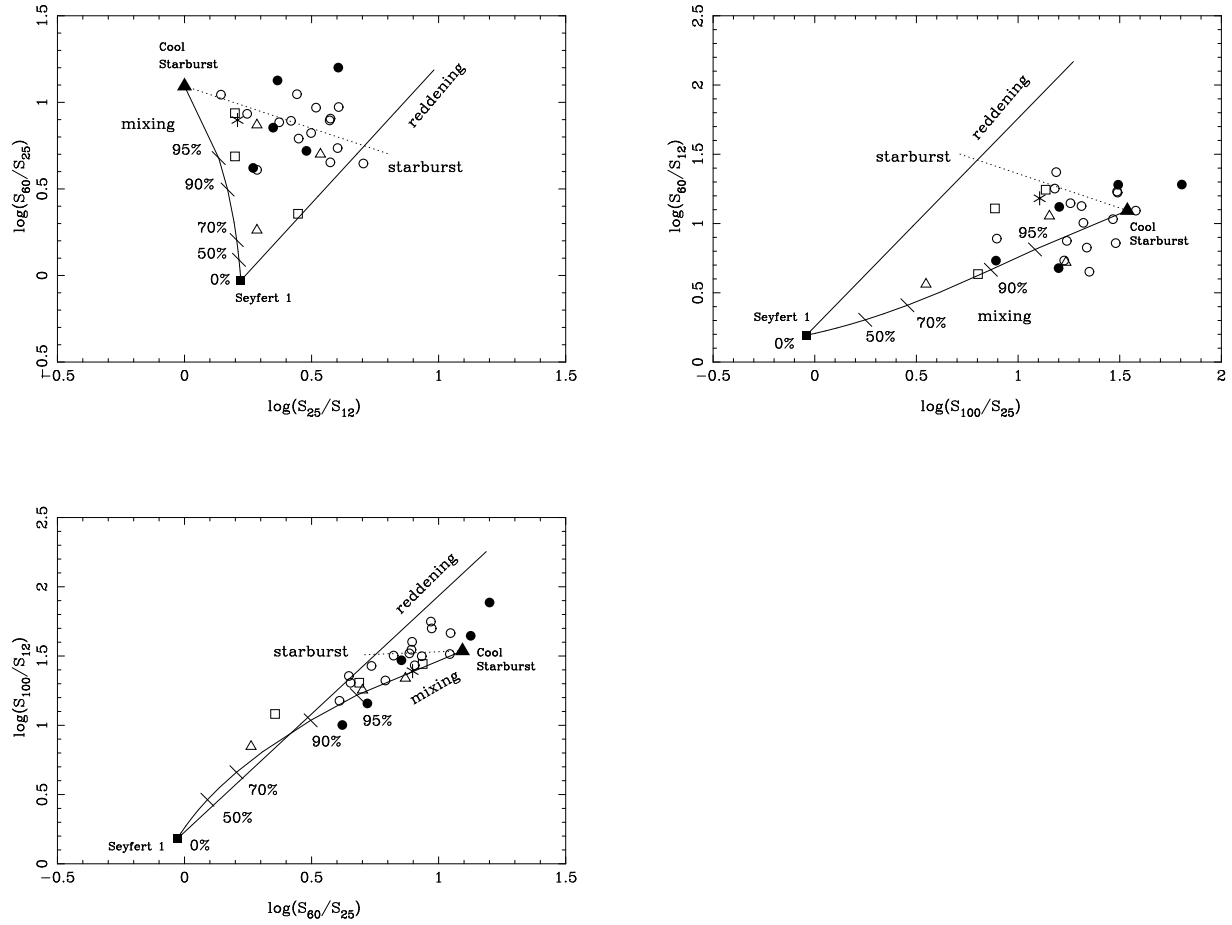


Fig. 3.— IR colour-colour diagrams of (a) $\log(S_{60}/S_{25})$ vs $\log(S_{25}/S_{12})$; (b) $\log(S_{60}/S_{12})$ vs $\log(S_{100}/S_{25})$; (c) $\log(S_{100}/S_{12})$ vs $\log(S_{60}/S_{25})$. The solid line is the reddening line that shows the effect of extinction on a typical Seyfert 1 (given by \blacksquare), the solid curve is the extreme mixing curve and the dotted line is an empirical starburst line from a “cool” starburst (given by \blacktriangle) to a “hot” starburst, following Dopita *et al.* (1998). The composite galaxies are shown as: \bullet – detected by PTI; \circ – not detected by PTI; $*$ – not observed with PTI. The reference galaxies from Table 1 are shown as: \triangle – starbursts and \square – Seyferts.

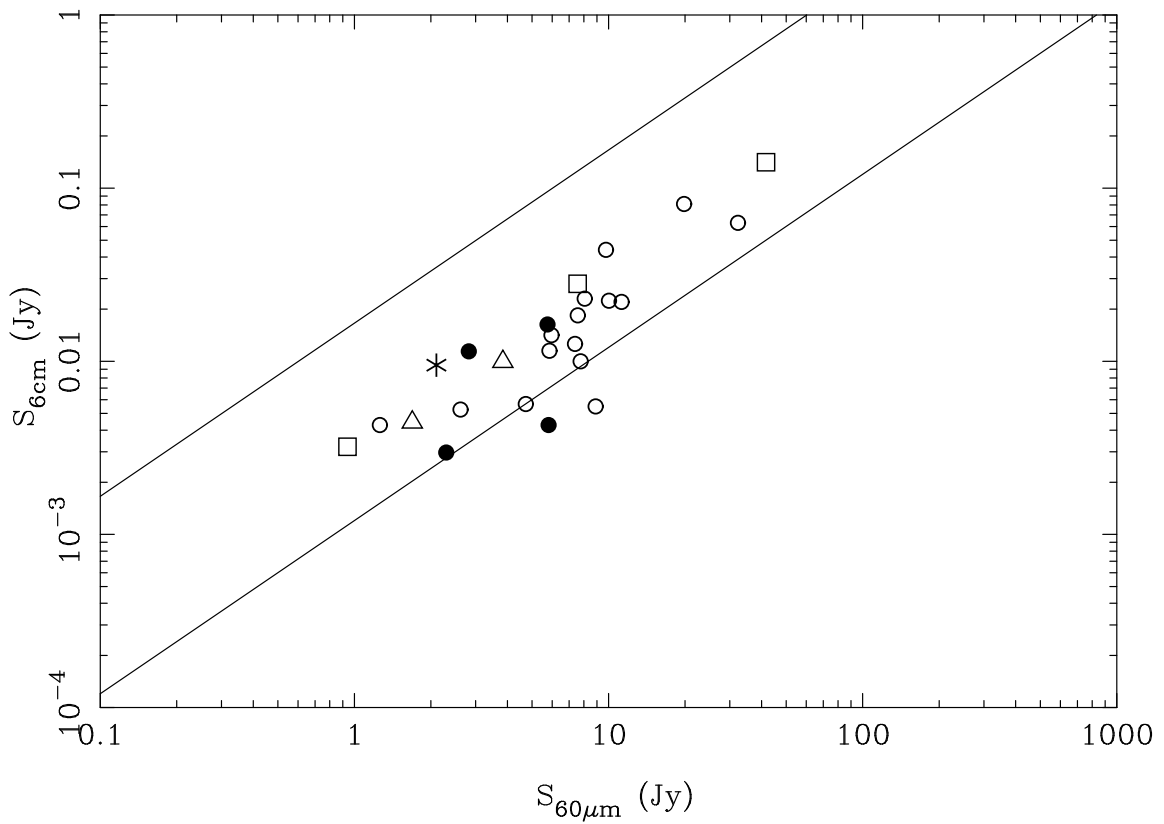


Fig. 4.— Radio-FIR correlation for our sample. The composite galaxies are shown as: \bullet – detected by PTI; \circ – not detected by PTI; $*$ – not observed with PTI. The reference galaxies from Table 1 are shown as: \triangle – starbursts and \square – Seyferts. The solid lines indicate the $\pm 3\sigma$ extent of the correlation found by de Jong (1985).

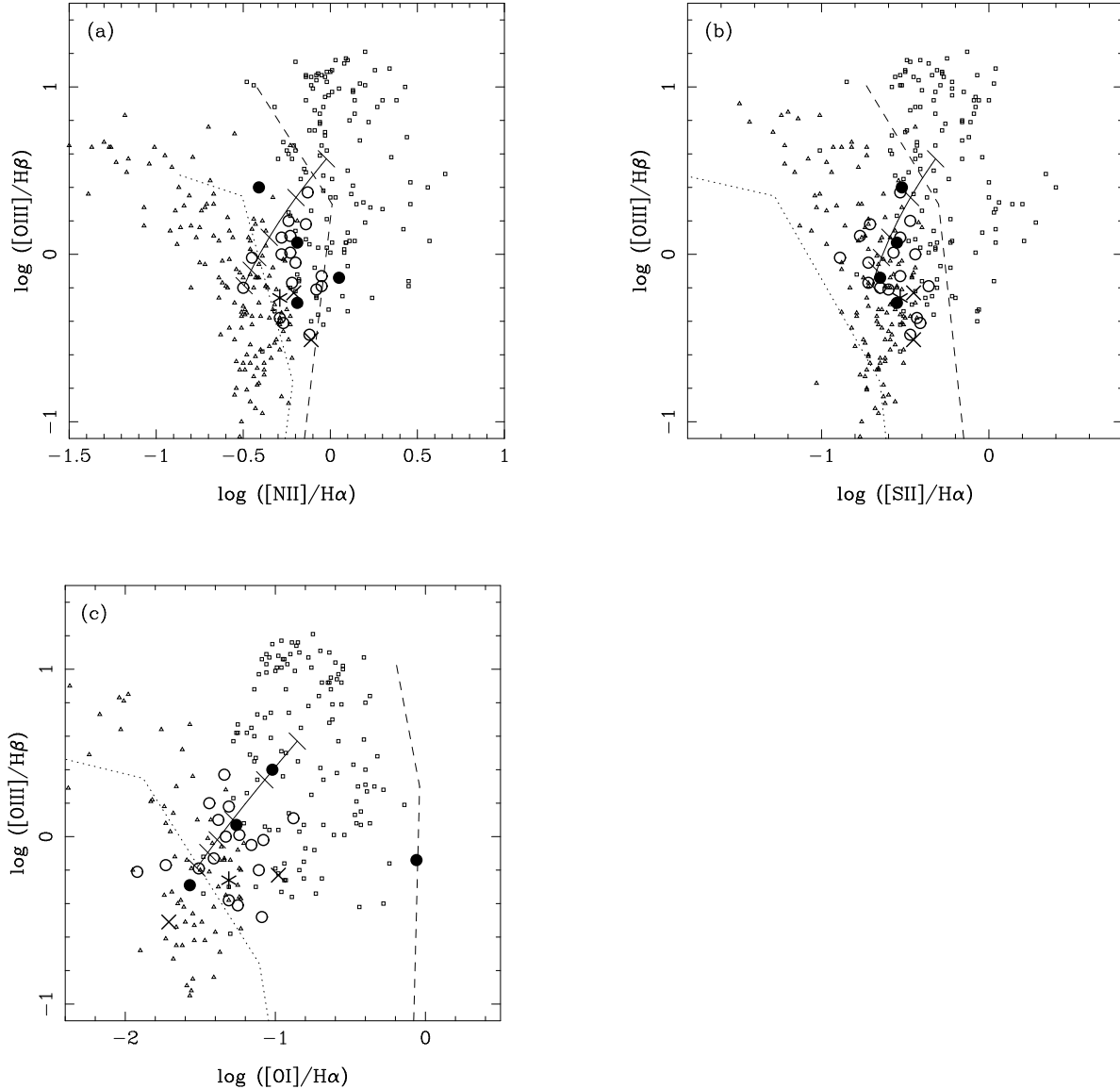


Fig. 5.— The optical diagnostic diagrams: (a) $[\text{O III}]/\text{H}\beta$ vs $[\text{N II}]/\text{H}\alpha$; (b) $[\text{O III}]/\text{H}\beta$ vs $[\text{S II}]/\text{H}\alpha$; (c) $[\text{O III}]/\text{H}\beta$ vs $[\text{O I}]/\text{H}\alpha$. Symbols have the following meaning: \triangle – starbursts and \square – AGNs from the literature (Veilleux & Osterbrock 1987 and references therein). The composite galaxies are shown as: \bullet – detected by PTI; \circ – not detected by PTI; \times – the two individual galaxies in the galaxy pair of ESO 550-IG025 (a compact core was detected with PTI directly between the two galaxies); $*$ – not observed with PTI. The dotted line is a starburst model and the dashed line is a power-law model from Paper 1. The solid curve is a mixing line with the tick marks from bottom to top, representing an AGN/starburst mix of 0%, 5%, 10%, 20%, 50% and 100% AGN. The end-points of the mixing curve are medians of the data for starburst and Seyfert galaxies.

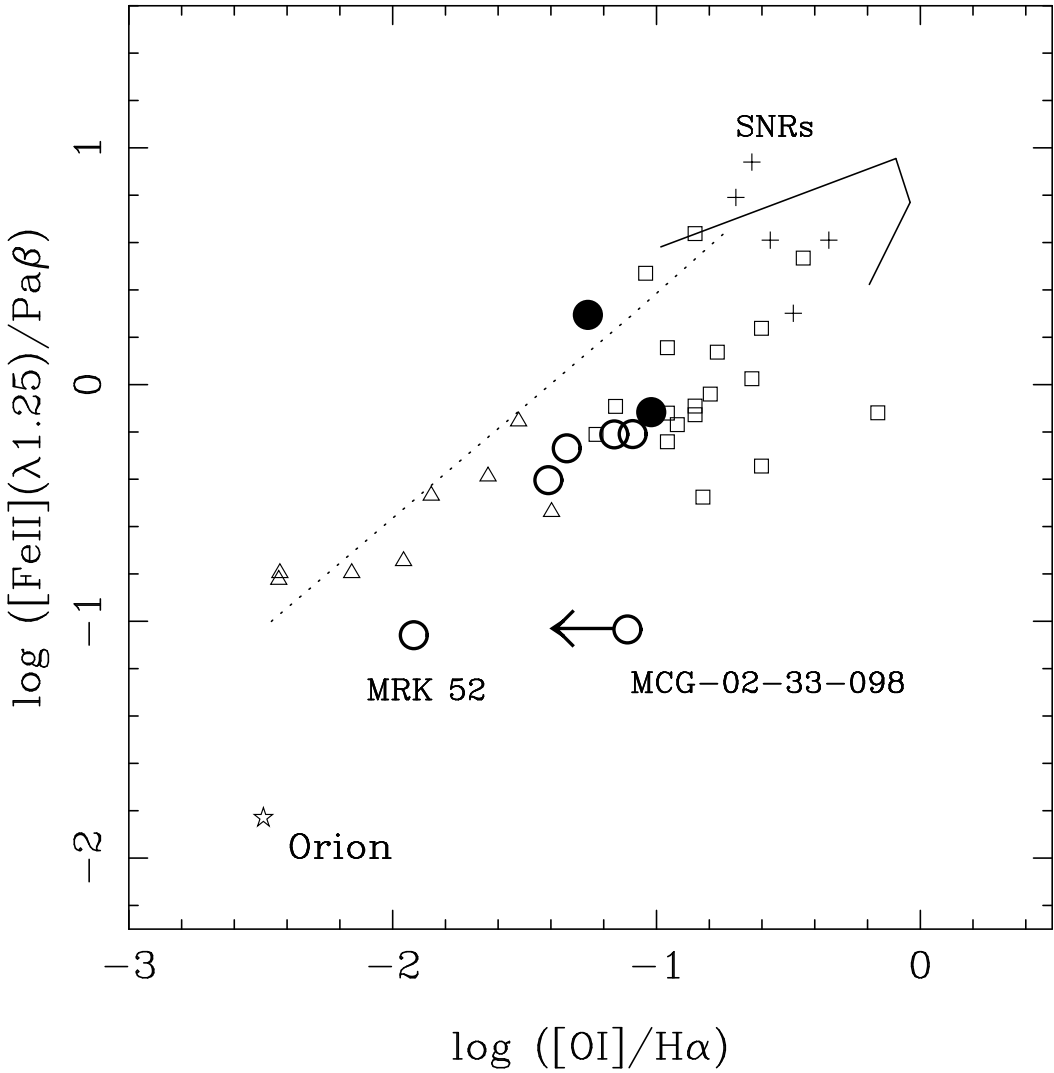


Fig. 6.— The $[\text{Fe II}](1.25 \mu\text{m})/\text{Pa}\beta$ vs $[\text{O I}]/\text{H}\alpha$ diagram with the starburst model (dashed line) and power-law model (solid line) from Paper 1. Symbols have the following meanings: \square – AGNs (Simpson *et al.* 1996); \triangle – starbursts (Mouri *et al.* 1990); $+$ – SNRs (Mouri *et al.* 1993). The Orion Nebula is also marked on the diagram (Mouri *et al.* 1993). The composite galaxies are shown as: \bullet – detected by PTI (Mrk 1344 and MCG+00-29-23); \circ – not detected by PTI. The optical line ratios are from the surveys of Veilleux & Osterbrock (1987), van den Broek *et al.* (1991), Ashby *et al.* (1995) and Veilleux *et al.* (1995).